DOI: 10.1002/adem.((please add manuscript number))

Crystallohydrate loaded Halloysite Nanocontainers for Thermal Energy Storage**

By *Xiaolei Zhu,* and *Dmitry Shchukin**

[*] *Prof. Dr. D. Shchukin, X. Zhu*
Peach Street
Stephenson Institute for Renewable Energy, L69 7ZF, UK
E-mail: D.Shchukin@liverpool.ac.uk

[**] *The work was supported by ERC Consolidator grant Enercapsule (647969) and ERC PoC grant Enerpaint (767173).*

((The mixture of crystallohydrate phase change materials (PCMs) $Na_2HPO_4{\cdot}12H_2O$ and $Na_2SO_4{\cdot}10H_2O$ is loaded into halloysite nanotubes (HNTs) by water bath sonication and impregnation under vacuum at 40 ˚C. It is the first time HNTs are applied as nanocontainers for crystallohydrate PCMs for thermal energy storage. The PCM retains well in the nanocontainers over the solid-liquid phase change, due to the electrostatic interaction between PCM and the inner space of HNTs as well as the nanoconfinement effect. No new covalent bonding is formed between PCM and HNTs in the composite. The crystal structure of the hydrated salts mixture does not change after loading into HNTs. With 67wt% effective loading of $Na_2HPO_4{\cdot}12H_2O$ and $Na_2SO_4{\cdot}10H_2O$ in 1:1 mass ratio, the nanocontainer composite exhibits the melting temperature of 35.8 ˚C and the melting enthalpy of 142 J g^{-1}. During the thermal cycling tests, it shows no phase separation and the thermal stability is well kept over 50 cycles. The PCM/HNTs nanocontainers can be considered as efficient nanoscaled energy storage units with great potential in practical applications.))

1. Introduction

Phase change materials (PCMs) are widely applied for thermal energy storage in building materials,[1,2] smart textiles,[3] and greenhouses.[4] Both organic and inorganic substances can

be used as PCMs. Organic PCMs including paraffin,[5] fatty acid[6] and glycols[7] have the disadvantages such as low thermal conductivity (about 0.2 W m^{-1} K^{-1}),[8] flammability and usually toxicity.[9] On the other hand, crystallohydrates, as the main family of inorganic PCMs, show higher thermal conductivity (0.5-0.7 W m^{-1} K^{-1}),[8] inflammability, non or slight toxicity,[10] low cost and often higher latent heat.[11] All these characteristics make crystallohydrates advantageous candidates as PCMs comparing to the organic PCMs.

Among vast variation of hydrated salts, $Na_2HPO_4 \cdot 12H_2O$ (disodium phosphate dodecahydrate, DHPD) is considered as attractive PCM due to high mass heat storage capacity of 256-281 J g^{-1}[12] and low melting temperature range of 35-44 ˚C.[13]

The problem of phase separation is considered as disadvantageous for inorganic PCMs, since it decreases the melting enthalpy of the material. There are several methods to solve it. One of them is to add thickening agents such as sodium polyacrylate to stop phase separation in the beginning.[14] However, the melting enthalpy retains only for maximum 10-15 thermal cycles due to the boundary interface appeared between PCM crystals and thickening agent. The microencapsulation of $Na_2HPO_4 \cdot 12H_2O$ into polymer shell by solvent-evaporation-precipitation method[15] can prevent phase separation, but no information on durability in thermal cyclings was given. The polymer shell formed during the solvent evaporation does not keep water content constant and the fabrication method is complicated.

In a recent research,[16] $Na_2HPO_4 \cdot 12H_2O$ has been mixed with $Na_2CO_3 \cdot 10H_2O$ to form eutectic hydrated salts (EHS). The eutectic mixture can effectively reduce phase separation of hydrated salts.[17,18] However, the phase change effects after thermal cycling were not discussed.

Composite PCMs attracted much attention during the last decade.[19–21] Due to the simple fabrication process by mixing PCMs with supporting material and often good thermal stability in the cycling tests, they are considered as an effective thermal energy storage tool.[22] Hydrated salts have been mixed with metal nanoparticles to form composite PCMs.[21,23]

Despite the improved thermal conductivity, the decreased heat storage capacity, high cost of metal nanoparticles, their corrosion and usually poor performance in cycling tests limit the application of hydrated salts/metal nanoparticles composites. Porous material such as expanded graphite (EG) has also been reported to form composites with $NaCH_3COO \cdot 3H_2O$[24,25] and $CaCl_2 \cdot 6H_2O$.[26] Haillot et al.[24] has compressed $NaCH_3COO \cdot 3H_2O$ directly with EG resulting in only one melting peak detected from the first thermal run. By adding carboxymethyl cellulose (CMC) as thickening agent, Shin et al.[25] obtained $NaCH_3COO \cdot 3H_2O$/EG composite retaining thermal properties after 5 cyclings. With large number of pores in micrometer range,[27] EG is actually not the optimal candidate to absorb hydrated salts and prevent them from leaking when they have liquid phase.

Halloysite nanotubes (HNTs) is natural mineral clay, which can be found across the world.[28] They have hollow cylinder morphology with a small inner lumen of 10-30 nm and a length up to tens of micrometers.[29] Easy accessibility, low-cost, non-toxicity as well as regular nanoconfinement and high specific area[28] have made HNTs widely used as nanoreactors,[30–32] adsorption materials[33] or nanocontainers for controlled release of functional materials.[28,32,34] In a few recent research works,[35,36] they have been used as supporting matrix for organic PCMs. The surface of HNTs is hydrophilic and it consists of inner and outer parts with different chemical composition. The inner surface of the lumen has a positive charge due to Al-OH groups, and the external surface is negative with siloxane (Si-O-Si) groups.[29] Till now, HNTs have not been reported as nanocontainers for encapsulation of inorganic crystallohydrate PCMs.

Our work demonstrates a novel and effective solution of phase separation problem and instability in thermal cyclings of crystallohydrates on the example of $Na_2HPO_4 \cdot 12H_2O$ mixed with $Na_2SO_4 \cdot 10H_2O$ (sodium sulfate decahydrate, SDH) to form binary eutectic hydrated salts mixture, and then loading the EHS into HNTs. As the nanoconfinement effect from HNTs may not completely inhibit the phase separation of $Na_2HPO_4 \cdot 12H_2O$, the eutectic

phenomenon of hydrated salts mixture is used as auxiliary. The effect of HNTs in the crystallohydrate/HNTs nanocontainer composite is also highlighted by comparing DHPD/HNTs with pure DHPD.

2. Results and Discussion

2.1. Thermal characterization of crystallohydrates loaded HNTs nanocontainer composites

To demonstrate the influence of HNTs on melting behaviour of hydrated salts, two groups of samples DHPD vs. DHPD/HNTs and 1DHPD:1SDH vs. 1DHPD:1SDH/HNTs were tested, as shown in **Figure 1**a. In the Supplementary Information Section, the correspondent DSC data are listed in **Table S1**a and the melting curve of SDH is shown in **Figure S1**. In the first group, $Na_2HPO_4 \cdot 12H_2O$ has two obviously separated big melting peaks at 42.6 °C and 51.9 °C, which indicates strong phase separation. The first peak is due to the melting of $Na_2HPO_4 \cdot 12H_2O$,[12] while the peak at 51.9 °C appears from the melting of $Na_2HPO_4 \cdot 7H_2O$.[10] In comparison, the DHPD/HNTs have a main peak at 42.4 °C from the melting of $Na_2HPO_4 \cdot 12H_2O$ and a small peak at 47.6 °C. DHPD/HNTs show a smaller melting temperature range than DHPD. The splitting of two melting peaks is much lower, confirming the phase separation of DHPD has been clearly reduced in the HNTs nanocontainer composite. This could result from the nano-confinement effect of HNTs. The diffusion of the hydrated salts is accelerated inside nanosized halloysite lumen,[37-40] leading to homogenization during the melting. In the second group, both hydrated salts mixture 1DHPD:1SDH and 1DHPD:1SDH/HNTs show one melting peak. The nanocontainer composite exhibits a slightly lower melting peak at 35.8 °C than the melting peak of hydrated salts mixture at 38.5 °C. The decrease of the melting temperature of hydrated salts inside

HNTs is also observed by the second peak of DHPD/HNTs composite. This could be also explained by the nano-confinement effect. As the surface energy of PCM increases in nanotubes, its melting temperature decreases accordingly.[41–44]

Figure 1b displays the melting behaviour of PCM/HNTs nanocontainer composite with different salt ratio. Hydrated salts mixture/HNTs show different melting temperature as compared to pure DHPD/HNTs and SDH/HNTs. The 3DHPD:1SDH/HNTs have separation of two melting peaks. The one at 35 °C is caused by the melting of the eutectic mixture, while the one at 46.9 °C could be attributed to the phase separation of the DHPD excess. As the ratio of SDH increases to 1DHPD:1SDH, only one melting peak at 35.8 °C is present, which

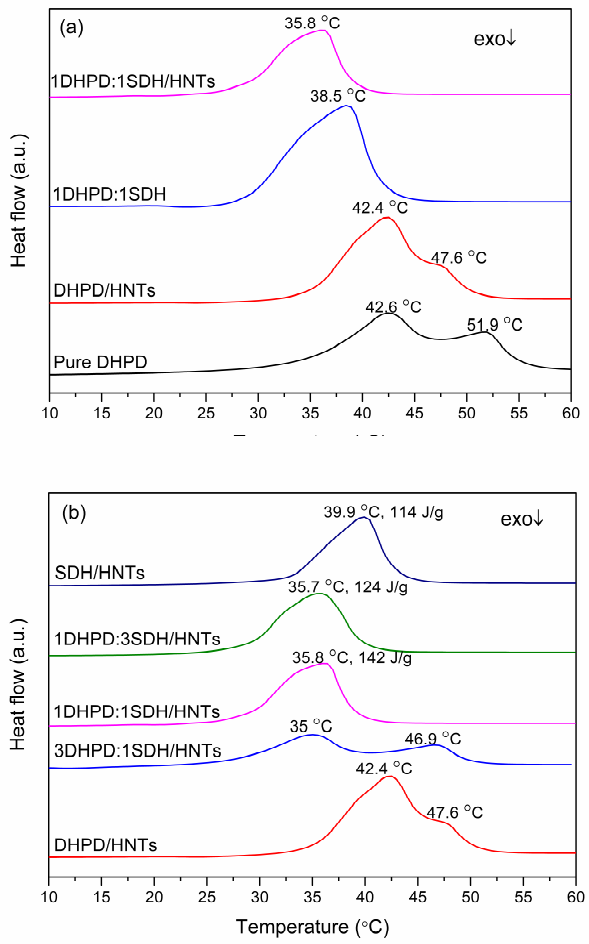

Figure 1. *a) Comparison of DSC melting curves of pure hydrated salts to correspondent hydrated salts/HNTs, b) DSC melting curves of hydrated salts/HNTs with different mass ratios of DHPD to SDH*

is the eutectic point of the mixture. The melting enthalpy is 142 J g^{-1}. 1DHPD:3SDH/HNTs also shows one melting peak at 35.7 °C, and the melting enthalpy is 124 J g^{-1}. The melting peak from the eutectic mixtures and the one from SDH excess could fuse together to form one broad peak. The lower melting enthalpy compared to 1DHPD:1SDH/HNTs should be attributed to the excess amount of SDH. For further investigation of the optimum loading in HNTs, the eutectic hydrated salts mixture 1DHPD:1SDH is selected.

2.2. Effect of the PCM loading on composite properties

Regarding different starting loading percentage of the hydrated salts, the melting behaviour of composite is shown in **Figure 2**, including correspondent melting point and melting enthalpy. All the composites consist of hydrated salts mixture with 1DHPD:1SDH mass ratio and have a consistent single melting peak at about 36 °C. The melting enthalpy of the composite increases with the loading percentage of hydrated salts mixture. Further, by comparing the increment of melting enthalpy per 1wt% increase of loading, it should be noticed that from 58wt% to 70wt% the rate is 3.6 J g^{-1} $wt\%^{-1}$, which is much higher than the one from 70wt% to

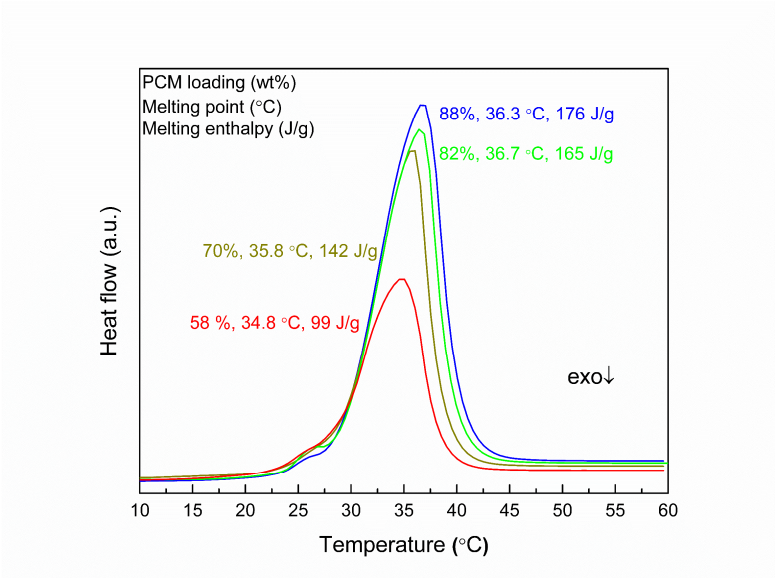

Figure 2. *DSC melting curves of PCM/HNTs nanocontainer composite with various loading of hydrated salts mixture (1DHPD:1SDH) as PCM*

82wt% (1.9 J g^{-1} $wt\%^{-1}$), and from 82wt% to 88wt% (1.8 J g^{-1} $wt\%^{-1}$). The hydrated salts loaded into the halloysite nanotubes can retain latent heat enthalpy much better than the ones absorbed on the surface or even not attached to HNTs, as the confined nanotube volume prevent the degradation of hydrated salts. Correspondently, the hydrated salts from 58wt% to 70wt% are loaded inside HNTs, while further increase of PCM content from 70wt% to 88wt% should locate largely outside HNTs. The much smaller increasing rates of the melting enthalpy indicates the formation of PCM aggregates outside HNT lumen over 70wt%.

The SEM images of HNTs and PCM-loaded HNTs nanocontainer composites with different loading are illustrated in **Figure 3**. Halloysite has the form of nanotubes (Figure 3a), with an average outer diameter of 70 nm. The dominant morphologies are long tubes with the length from 800 nm to 1 µm, although some short tubes below 200 nm are observed. With 58wt% of loaded hydrated salts (Figure 3b), the composite shows similar morphology as unloaded HNTs. Separated nanotubes can be observed. The ends of most nanotubes are blocked with loaded hydrated salts. Composite with 70wt% loading (Figure 3c) also maintains the

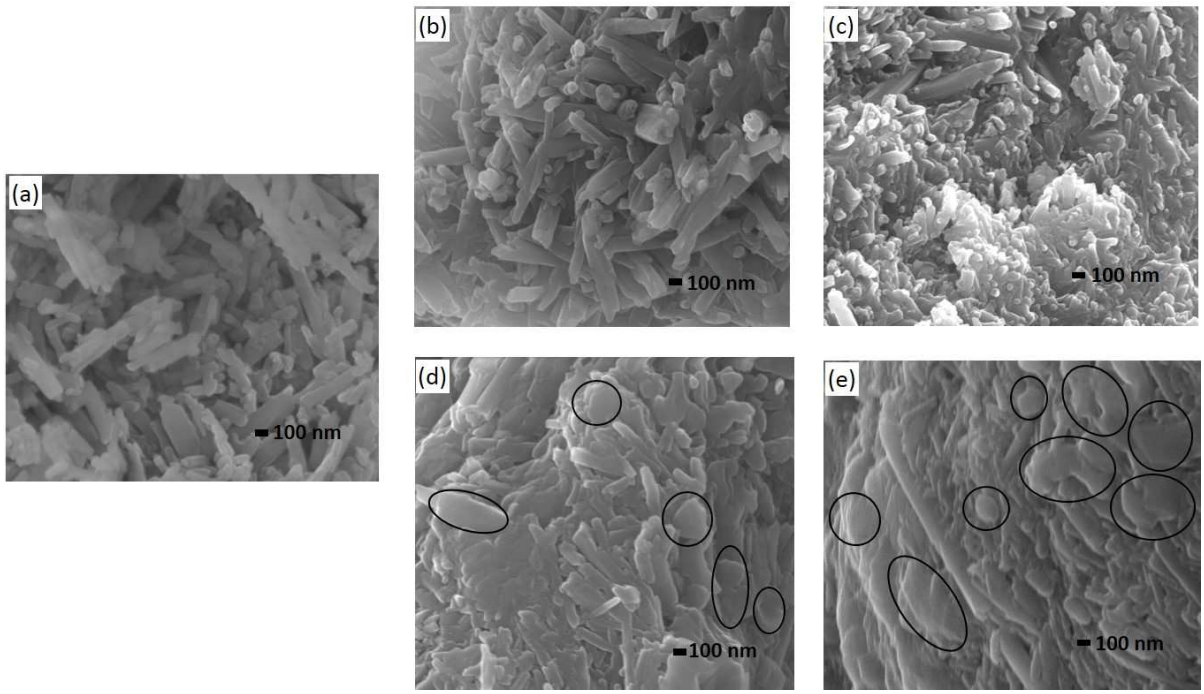

Figure 3. *SEM images of (1DHPD:1SDH)/HNTs nanocontainer composite at the loading percentage of: a) pure HNTs, b) 58wt%, c) 70wt%, d) 82wt%, e) 88wt% PCM. Circles indicate unloaded PCMs*

nanotubular morphology with increased number of the aggregates. When the loading rises to 82wt% (Figure 3d), some irregular block material is observed besides the nanotube aggregates, indicating existence of hydrated salts crystals outside nanotubes. For the sample with 88wt% PCM content (Figure 3e), more irregular block material randomly appeared among or on the surface of nanotubes, showing oversaturation of the loading.

To determine the optimum PCM loading into halloysite nanocontainers, thermal cycling tests of samples with 58%, 70wt%, 82wt% and 88wt% loading were carried out. Changes of the melting enthalpy in the heat uptake/release cycles are displayed in **Figure 4**. At 88wt% loading, the melting enthalpy decreases rapidly after 10 cycles and the decrement reaches 52% after 33 cycles. Composite with 82wt% of hydrated salts is relatively stable for 33 cycles, and start to degrade after that. The melting enthalpy reduces by 43% after 50 cycles. On the contrary, the one with 70wt% loading shows the best thermal stability. The melting enthalpy change is only 7% after 50 cycles. Sample with 58 wt% loading also shows stability for 50 cycles, but the melting enthalpy is much lower than the 70 wt%. So the 70 wt% loading sample is used for further characterizations in this paper.

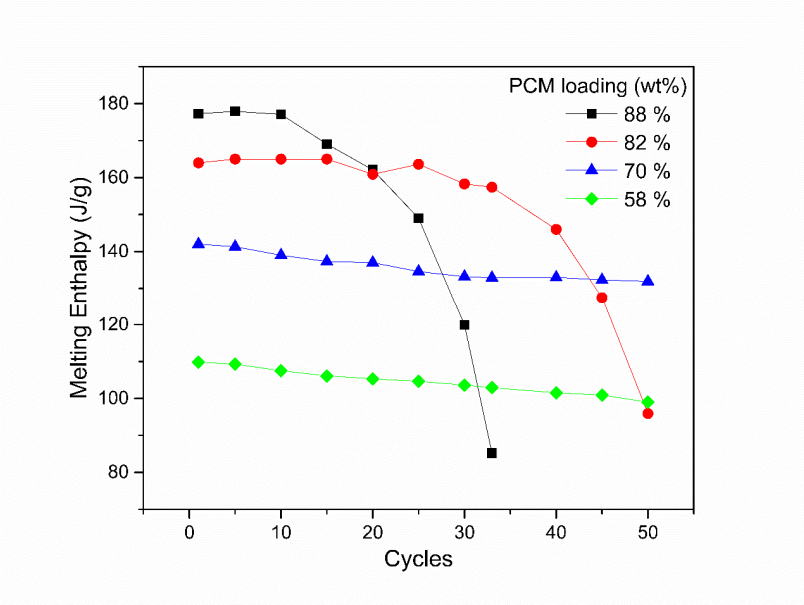

Figure 4. *Melting enthalpies of (1DHPD:1SDH)/HNTs composites with various loadings vs. numbers of heat uptake/release cycles*

2.3. Cycling properties of PCM/HNTs nanocontainer composite

The DSC curves of hydrated salts mixture and PCM/HNTs nanocontainer composite during 50 melting/freezing cycles are displayed in **Figure 5**. The summary of the correspondent DSC data can be seen in **Table S2**, Electronic Supplementary Information Section. The hydrated salts mixture has a melting point of 38.5 °C and melting enthalpy of 211 J g^{-1} during the first cycle. It shows a certain stability for the first twenty cycles due to the eutectic effect. After 20 cycles, the down shift of melting temperature becomes more evident and the melting enthalpy reduces rapidly with increasing cycle number. The melting point shift reaches 2.3 °C and the melting enthalpy reduces by 21 J g^{-1} after 30 cycles, following 5.3 °C and 83 J g^{-1} reduction after 50 cycles, which takes over 39.3% of the original melting enthalpy.

PCM/HNTs nanocontainer composite exhibits a melting point of 35.8 °C, which is lower than the pure hydrated salts mixture. The melting enthalpy is 67% of the hydrated salts mixture. Since HNTs does not have melting behaviour, the effective loading yield of the composite can thus be calculated as 67wt%. [45] It is similar to the starting loading percentage of 70wt%. The hydrated salts mixture keeps its melting enthalpy efficiently in the composite after the halloysite loading and drying. The composite demonstrates better thermal stability than pure hydrated salts mixture in heat uptake/release cycles. The melting temperature shift is only 0.9 °C, and the melting enthalpy decrease is 10 J g^{-1} after 50 cycles, which is only 7% of the starting value. The nano-confinement effect from HNTs evidently inhibits phase separation and PCM degradation during thermal cyclings.

Turbulence in freezing temperature is observed for both hydrated salts mixture and nanocontainer composite during cyclings. This could be attributed to the slow nucleation process for crystallohydrate PCMs. The hydrated salts start to nucleate at slightly different temperature during each cycle, and the process of heat release does not have a uniform rate for all nanotubes because of their difference in length, so the freezing peak can vary between

1 °C to 6 °C. It should be also noticed, the freezing enthalpy of the pure hydrated salts mixture decreases rapidly after 50 cycles, which is due to the phase separation effect.[46] In comparison, the freezing enthalpy of the nanocontainer composite does not show obvious change during cyclings. This proves again the phase separation is eliminated inside HNTs composite. It is assumed, that a relatively ordered crystal structure could be generated repeatedly within a confined space of halloysite lumen.

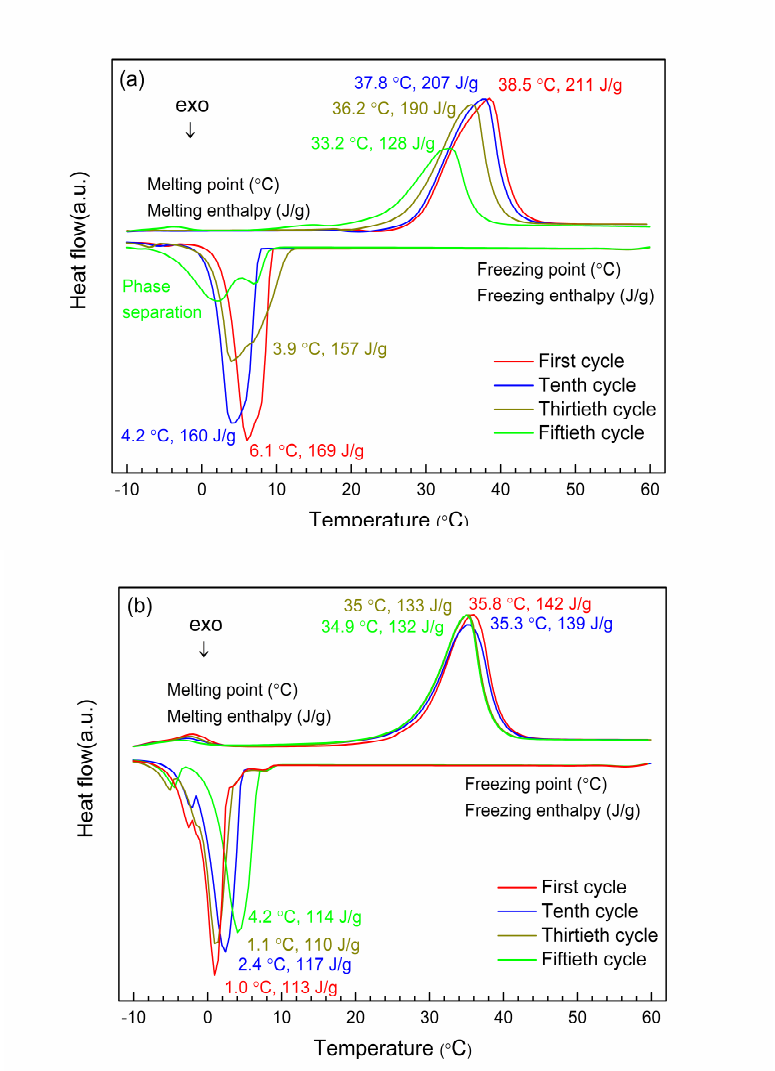

Figure 5. *a) Thermal cycling tests of hydrated salts mixture (1DHPD:1SDH) for 50 cycles, b) (1DHPD:1SDH)/HNTs nanocontainer composite for 50 cycles*

The stability of encapsulated PCM during heating/cooling cycles can be visually seen in **Figure 6**, where images of hydrated salts mixture and encapsulated hydrated salts nanocontainer composite before and after heating at 60 ˚C are displayed. The melting

temperature of hydrated salts mixture is about 36 ˚C. While the water leakage is obvious for pure hydrated salts mixture, the PCM-loaded nanocontainers keep a stable powder form and no liquid leakage is observed after heating to 60 ˚C.

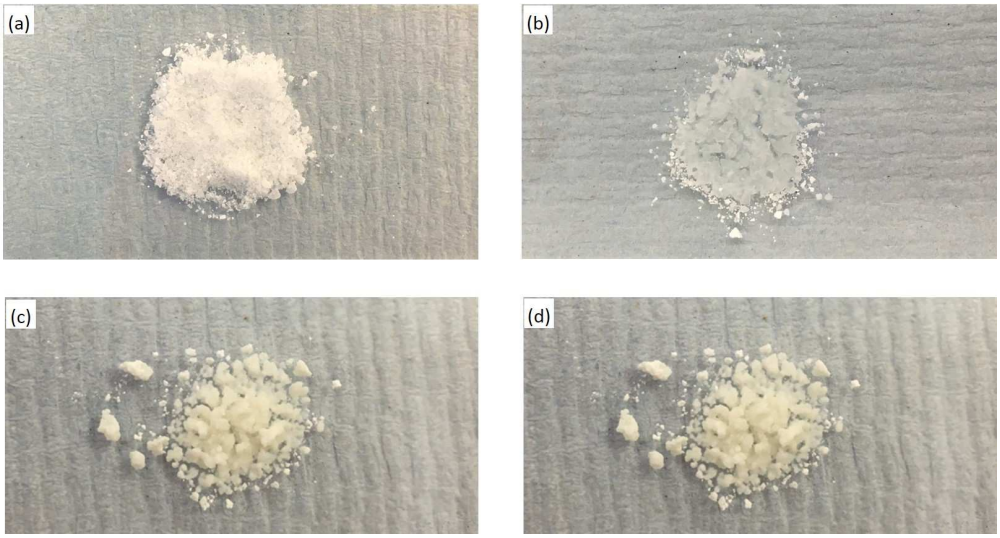

Figure 6. *Photos of hydrated salts mixture (1DHPD:1SDH) before a) and after b) heating, (1DHPD:1SDH)/HNTs composite before c) and after d) heating at 60 ˚C*

2.4. Structural characterization of PCM/HNTs nanocontainer composite

Figure 7a shows the TEM images of HNTs. They are hollow nanotubes with average inner diameter of 30 nm, and the average shell thickness of 20 nm. The average outer diameter is 70 nm, and the tube length ranges from 200 nm to 1 µm, in accordance with the observations from the SEM images (Figure 3a). The EDX measurement detected Si, Al, O elements in pure HNTs (Figure 7b). This corresponds to the unit formula for halloysite as $Al_2Si_2O_5(OH)_4$.[29] The TEM images of crystallohydrates loaded HNTs are displayed in Figure 7c. The inner lumen of the HNTs is filled with hydrated salts. The EDX spectrum from Figure 7d shows the presence of P, S, Na elements in the composite, which appear from the crystallohydrates. Combining the observation from the TEM images and the EDX measurement, it can be confirmed that hydrated salts mixture is located inside HNTs in the hydrated salts/HNTs nanocontainer composite.

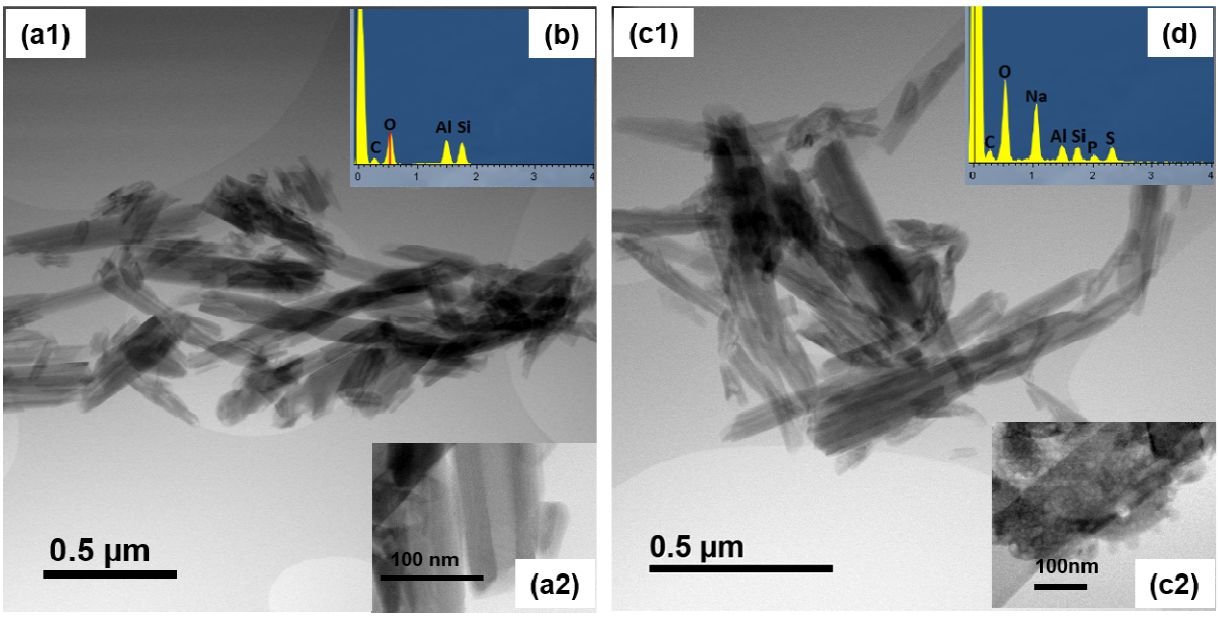

Figure 7. *TEM images of a) HNTs, c) PCM-loaded HNTs, EDX spectra of b) HNTs, d) PCM-loaded HNTs*

The FTIR spectra of hydrated salts mixture, PCM/HNTs and pure HNTs are displayed in **Figure 8**. HNTs show the characteristic absorption peaks at 3625 cm^{-1} and 3694 cm^{-1}, which correspond to the vibration of two alumina stretching bands.[47] In the spectrum of the hydrated salts, the peak at 618 cm^{-1} is assigned to the asymmetric bending vibration of SO_4 group.[48] The peak at 861 cm^{-1} corresponds to the symmetric vibration of P-OH.[49] The P-O bonding shows two obvious peaks, one at 985 cm^{-1} due to the symmetric vibration, and the other at 1098 cm^{-1} from the asymmetric vibration.[50]

In PCM/HNTs composite the vibration peaks of alumina from halloysite are found without any shift, indicating the chemical composition of the halloysite does not change in the composite. Also the typical peaks from S-O and P-OH are detected at fast the same wavenumbers as for hydrated salts mixture. However, both peaks of P-O bond show a shift from 985 to 912 cm^{-1} and from 1098 to 1031 cm^{-1}, which can be attributed to the electrostatic interactions between negatively charged P-O bonds and positively charged alumina layer in the lumen of HNTs. This explains hydrated salts are predominantly absorbed inside positively charged alumina inner space, but not on the negatively charged silica outer surface of HNTs.

The stretching vibration of the alumina layer is not influenced by the weak electrostatic interaction from the hydrated salts, which should be due to the strong network structure in the layer. In the FTIR spectra, all characteristic peaks of halloysite and hydrated salts mixture are displayed, and no new peaks are found. This could be considered as evidence, that no new covalent chemical bonding is formed between hydrated salts and halloysite as nanocontainer material.

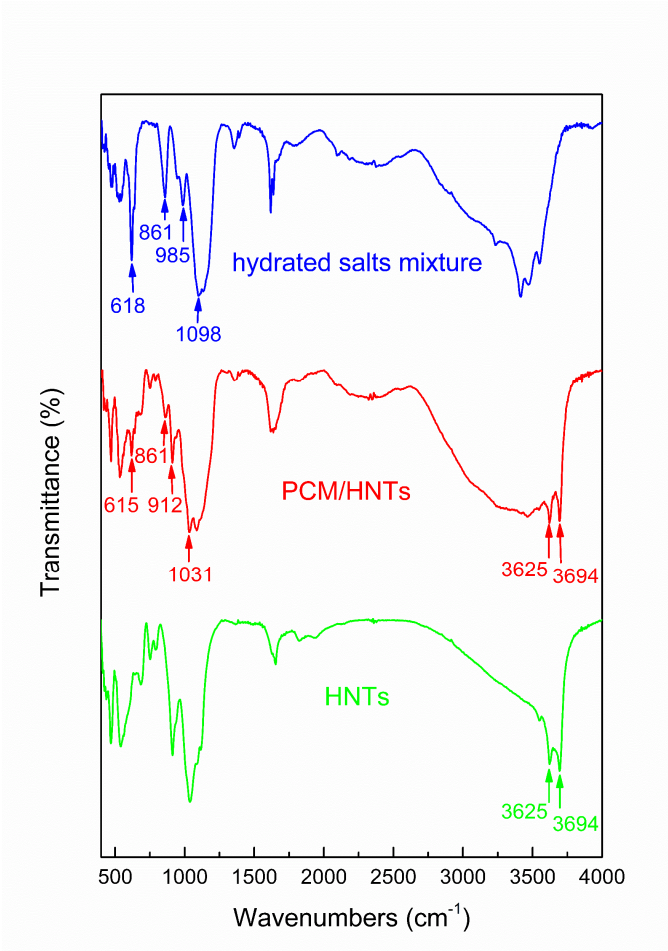

Figure 8. *FTIR spectra of hydrated salts mixture (1DHPD:1SDH), (1DHPD:1SDH)/HNTs nanocontainer composite and pure HNTs*

Figure 9 shows the comparison of the XRD patterns from the PCM/HNTs nanocontainer composite, HNTs and hydrated salts mixture. HNTs exhibit a characteristic peak at 11.9 °, which is assigned to the multiwall nano-tubular structure.[51] The same diffraction peak is observed in the XRD pattern of hydrated salts /HNTs, indicating the same tube wall structure

of HNTs is preserved in the nanocontainer composite. Other sharp peaks at 26.4 °, 24.8 ° and 19.8 ° from HNTs have also been found in the nanocontainer composite. The diffraction peaks of hydrated salts mixture are also observed in the same place in the nanocontainer composite, confirming the presence of the hydrated salts mixture and the maintenance of their crystal structures in the nanocontainer composite. Moreover, the nanocontainer composite after heating to 60 °C and cooling shows the same XRD pattern as the sample before heating. It demonstrates the crystal structure of the nanocontainer composite sample does not change during heating.

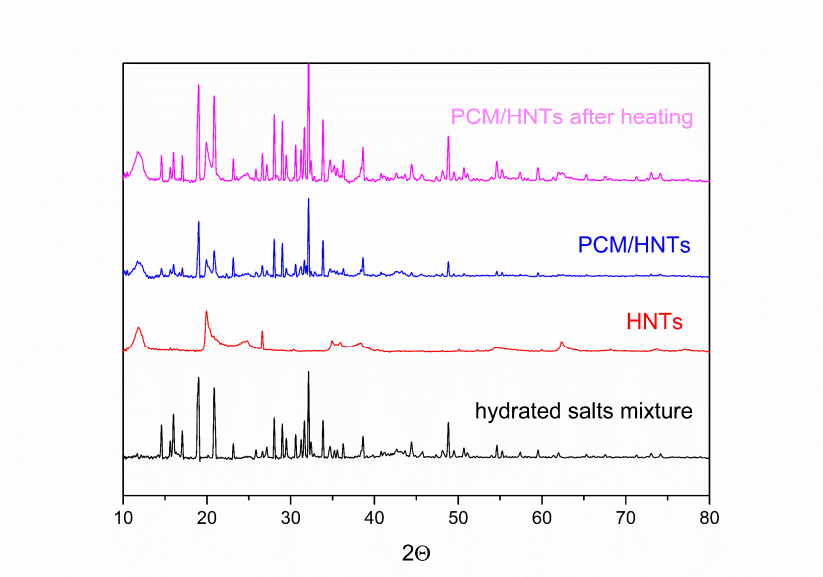

Figure 9. *XRD patterns of hydrated salts mixture (1DHPD:1SDH), HNTs and (1DHPD:1SDH)/HNTs nanocontainer composite before and after heating at 60 °C*

3. Conclusion

In this study, a eutectic crystallohydrate PCM/HNTs nanocontainer composite system was fabricated to eliminate the phase separation of crystallohydrates as phase change materials as well as to improve their thermal stability over phase change cyclings. The mixture of $Na_2HPO_4 \cdot 12H_2O$ (DHPD) and $Na_2SO_4 \cdot 10H_2O$ (SDH) was selected as crystallohydrate PCM because of their ability to form stable eutectic hydrated salts with low melting temperature

(<40˚C) suitable for domestic heat region. HNTs as nanocontainers have the advantages of low-cost and easy accessibility. They have long nanotubular morphology with the average inner diameter of 30 nm, the average shell thickness of 20 nm and the tube length ranges from 200 nm to 1 µm. This provides good nano-confinement effect on the loaded crystallohydrate PCMs, which can be proved by the improved phase change performance and cycling stability. Meanwhile, the proper ratio of inner diameter to shell thickness endows HNTs as nanocontainers high loading property as well as structure stability. Due to the vacuum impregnation process and the electrostatic interaction between Al-OH from the inner alumina layer and P-O from eutectic hydrated salts mixture, PCM was encapsulated into the lumen of HNTs. The composite with 67wt% loading of DHPD and SDH in 1:1 mass ratio exhibits no phase separation during heat uptake/release. Its melting temperature retains around 35 °C and the melting enthalpy decreases only by 7% from 142 J g^{-1} to 132J g^{-1} after 50 cycles. The structural characterization shows the crystallohydrates in HNTs nanocontainer composite have the same IR and XRD pattern as their pure form and no new chemical bonding is formed between crystallohydrates and HNTs. During the heating to 60 °C, the morphology of the nanocontainer composite keeps stable and its crystalline structure remains unchanged after cooling. In general, the encapsulation of eutectic crystallohydrates in HNTs as nanocontainers can be considered as effective strategy to address two common problems when inorganic crystallohydrates are used as PCMs for thermal energy storage, namely the phase separation and poor cycling stability. The employment of the HNTs with low cost and easy accessibility as supporting nanomaterial, the simple fabrication process, as well as the non-toxic property of all chemicals included in the composite, make the PCM/HNTs nanocontainer composite system economically efficient and environment-friendly. The proper melting temperature together with high melting enthalpy render the system big potential in applications of the latent heat storage in low temperature range.

4. Experimental Section

Materials: Sodium sulfate decahydrate ($Na_2SO_4 \cdot 10H_2O$, SDH, purity > 99%, melting point 32.4 °C) was purchased from Sigma, USA. Sodium phosphate dibastic dodecahydrate ($Na_2HPO_4 \cdot 12H_2O$, DHPD, purity > 99%) was purchased from Sigma, Germany. Halloysite nanoclay ($H_4Al_2O_9Si_2 \cdot 2H_2O$), in the form of nanopowder, was supplied by Aldrich, USA. All materials were used as purchased without further purification. Milli Q water was applied as a solvent media.

Preparation of PCM-loaded HNTs nanocontainer composite (PCM/HNTs): The PCM/HNTs were prepared by sonication and impregnation of concentrated hydrated salts solutions under vacuum. To determine the optimal composition and mass ratio of hydrated salts loaded in HNTs, $Na_2HPO_4 \cdot 12H_2O$ and $Na_2SO_4 \cdot 10H_2O$ mixtures (7 g) containing 0, 25, 50, 75 and 100wt% of $Na_2HPO_4 \cdot 12H_2O$ were dissolved in deionized H_2O (3 mL) at 40 °C. Halloysite (3 g) was added to the solution forming a white suspension. Series of composites containing hydrated salts (7 g) and halloysite (0.5, 1, 1.5, 3, 5, 7 g) were also prepared for investigation of the loading capacity of halloysite nanocontainers. The suspension was sonicated (VWR Ultrasonic Cleaner USC 500TH, output 100 W) at 40 °C for 30 minutes. A homogeneous white pulpy mixture was obtained after sonication. Then, the mixture was put into the vacuum oven at 40 °C. To achieve better impregnation of the PCMs into the halloysite lumen, the samples were first put under vacuum for 10 min, then exposed to the air at room temperature for 10 min. This process was repeated two times. In the last step, the samples were cooled at 4 °C for 30 minutes and dried in desiccator at room temperature for 2 days until the weight was constant.

Characterization: The morphology of the samples was characterized by scanning electron microscopy (SEM) and transmission electron microscopy (TEM). SEM images were recorded by JSM-7001F (JEOL Japan) setup. The samples were sputter coated by 100 nm chromium

layer before measuring. TEM measurements were operated on STEM-2100F (JEOL Japan) with STEM mode at 200 kV. The average diameter, inner diameter and shell thickness of the HNTs were calculated from 100 measurements. Energy-dispersive X-ray spectroscopy (EDX) was applied for elemental analysis. The chemical composition was characterized by Fourier transform infrared spectroscopy (FTIR) using TENSOR II instrument (Bruker, Germany) with all reflective diamond ATR. The transmittance mode was recorded from 400 to 4000 cm^{-1} as the result of 64 consecutive scans. The crystal structure of the samples was analysed by X-ray diffraction (XRD, Bruker diffractometer with CuK_a radiation). The diffraction data were recorded in the range of 5-60 ° with the scan speed of 1 ° min^{-1}. The thermal properties including cycling tests were characterized by differential scanning calorimeter (DSC, 214 NETZSCH, Germany). The measurements were undertaken in the temperature range from -20 to 70 °C with the ramp of 10 °C/min under nitrogen atmosphere. The thermal gravimetric (TGA) measurements were recorded from 22 to 200 °C with a heating rate of 5 °C min^{-1} under nitrogen atmosphere using STA PT-1000 (LINSEIS, Germany).

[1] A. de Gracia, L. F. Cabeza, *Energy Build.* **2015**, *103*, 414.

[2] T. Khadiran, M. Z. Hussein, Z. Zainal, R. Rusli, *Renew. Sustain. Energy Rev.* **2016**, *57*, 916.

[3] S. Mondal, *Appl. Therm. Eng.* **2008**, *28*, 1536.

[4] F. Berroug, E.K. Lakhal, M. El Omari, M. Faraji, H. El Qarnia, *Energy Build.* **2011**, *43*, 3027.

[5] M. Akgün, O. Aydın, K. Kaygusuz, *Energy Convers. Manag.* **2007**, *48*, 669.

[6] A. Sari, K. Kaygusuz, *Sol. Energy* **2001**, *71*, 365.

[7] P. M. Gilart, Á.Y. Martínez, M. G. Barriuso, C. M. Martínez, *Sol. Energy Mater. Sol. Cells* **2012**, *107*, 205.

[8] B. Zalba, J. M. Marin, L. F. Cabeza, H. Mehling, *Appl. Therm. Eng.* **2003**, *23*, 251.

[9] A. Sharma, V. V. Tyagi, C.R. Chen, D. Buddhi, *Renew Sust Energ Rev.* **2009**, *13*, 318.

[10] M. M. Farid, A. M. Khudhair, S. A. K. Razack, S. Al-Hallaj, *Energy Convers. Manag.* **2004**, *45*, 1597.

[11] L. F. Cabeza, A. Castell, C. Barreneche, A. Gracia, A. I. Fernandez, *Renew Sust Energ Rev.* **2011**, *15*, 1675.

[12] S. D. Sharma, H. Kitano, K. Sagara, *Res. Rep. Fac. Eng. Mie Univ.* **2004**, *29*, 31.

[13] H. Mehling, L. F. Cabeza, *Heat and Cold Storage with PCM. An up to Date Introduction into Basics and Applications,* Springer, Berlin, Germany **2008**, p. 11.

[14] X. Z. Lan, Z. C. Tan, D. T. Yue, Q. Shi, C. G. Yang, *Chinese J. Chem.* **2007**, *25*, 921.

[15] F. Salaün, E. Devaux, S. Bourbigot, P. Rumeau, *Carbohydr. Polym.* **2010**, *79*, 964.

[16] Y. Liu, Y. Yang, *Appl. Therm. Eng.* **2017**, *112*, 606.

[17] G. A. Lane, *Int. J. Ambient Energy* **1980**, *1*, 155.

[18] N. Yoneda, S. Takanashi, *Sol. Energy* **1978**, *21*, 61.

[19] M. M. Kenisarin, K. M. Kenisarina, *Renew. Sustain. Energy Rev.* **2012**, *16*, 1999.

[20] A. Trigui, M. Karkri, C. Boudaya, Y. Candau, L. Ibos, *Compos. Part B Eng.* **2013**, *49*, 22.

[21] X. Li, Y. Zhou, H. Nian, X. Zhang, O. Dong, X. Ren, J. Zeng, C. Hai, Y. Shen, *Energy & Fuels* **2017**, *31*, 6560.

[22] P. Zhang, X. Xiao, Z.W. Ma, *Appl. Energy* **2016**, *165*, 472.

[23] M. Chieruzzi, A. Miliozzi, T. Crescenzi, L. Torre, J.M. Kenny, *Nanoscale Res. Lett.* **2015**, *10*, 273.

[24] D. Haillot, V. Goetz, X. Py, M. Benabdelkarim, *Sol. Energy* **2011**, *85*, 1021.

[25] H. K. Shin, M. Park, H.-Y. Kim, S.-J. Park, *Appl. Therm. Eng.* **2015**, *75*, 978.

[26] Z. Duan, H. Zhang, L. Sun, Z. Cao, F. Xu, Y. Zou, H. Chu, S. Qiu, C. Xiang, H. Zhou, *J. Therm. Anal. Calorim.* **2014**, *115*, 111.

[27] H. N. Wang, Y. P. Zheng, F. Y. Kang, *J. Inorg. Mater.* **2003**, *18*, 606.

[28] Y. M. Lvov, D. G. Shchukin, H. Möhwald, R. R. Price, *ACS Nano* **2008**, *2*, 814.

[29] E. Joussein, S. Petit, J. Churchman, B. Theng, D. Righi, B. Delvaux, *Clay Miner.* **2005**, *40*, 383.

[30] D. G. Shchukin, G. B. Sukhorukov, R. R. Price, Y. M. Lvov, *Small* **2005**, *1*, 510.

[31] E. Abdullayev, R. Price, D. Shchukin, Y. Lvov, *ACS Appl. Mater. Interfaces* **2009**, *1*, 1437.

[32] D. Fix, D. V. Andreeva, Y. M. Lvov, D. G. Shchukin, H. Möhwald, *Adv. Funct. Mater.* **2009**, *19*, 1720.

[33] M. Zhao, P. Liu, *Microporous Mesoporous Mater.* **2008**, *112*, 419.

[34] L. Fu, H. Yang, A. Tang, Y. Hu, *Nano Res.* **2017**, *10*, 2782.

[35] D. Mei, B. Zhang, R. Liu, Y. Zhang, J. Liu, *Sol. Energy Mater. Sol. Cells* **2011**, *95*, 2772.

[36] W. Liang, Y. Wu, H. Sun, Z. Zhu, P. Chen, B. Yang, A. Li, *RSC Adv.* **2016**, *6*, 19669.

[37] S. M. Chathoth, E. Mamontov, P. F. Fulvio, S. M. Chathoth, E. Mamontov, Y. Huang, W.K. Kin, *EPL.* **2012**, *97*, 66004.

[38] S. Interaction, S. Yashonath, P. Santikary, *J. Phys. Chem.* **1994**, *98*, 6368.

[39] A. Striolo, *Nano Lett.* **2006**, *6*, 633.

[40] E. G. Derouane, J. B. Nagy, C. Fernandez, E. Laurent, P. Maljean, *Appl. Catal.* **1988**, *40*, L1.

[41] W. H. Qi, M. P. Wang, *J. Mater. Sci. Lett.* **2001**, *21*, 1743.

[42] K. K. Nanda, S. N. Sahu, S. N. Behera, *Phys. Rev. A* **2002**, *66*, 013208.

[43] E. Roduner, *Chem. Soc. Rev.* **2006**, *35*, 583.

[44] M. Zhang, M. Efremov, F. Schiettekatte, E. Olson, A. Kwan, S. Lai, T. Wisler, J.E. Greene, L.H. Allen, *Phys. Rev. B* **2000**, *62*, 10548.

[45] L. Geng, S. Wang, T. Wang, R. Luo, *Energy Fuels.* **2016**, *30*, 6153.

[46] S. Cantor, *Thermochim. Acta* **1979**, *33*, 69.

[47] V. C. Farmer, J. D. Russell, *Spectrochim. Acta* **1964**, *20*, 1149.

[48] L. Czuchajowski, S. Duraj, M. Kucharska, *J. Mol. Struct.* **2009**, *34*, 187.

[49] M. Mello, B. Vidal, *PLoS One* **2012**, *7*, e43169.

[50] M. K. Trivedi, A. Branton, D. Trivedi, G. Nayak, K. Bairwa, S. Jana, *J. Chromatogr. Sep. Tech.* **2015**, *6*, 1000282.

[51] E. Joussein, S. Petit, B. Delvaux, *Appl. Clay Sci.* **2007**, *35*, 17.

Figure 1. a) Comparison of DSC melting curves of pure hydrated salts to correspondent hydrated salts/HNTs, b) DSC melting curves of hydrated salts/HNTs with different mass ratios of DHPD to SDH

Figure 2. DSC melting curves of PCM/HNTs nanocontainer composite with various loading of hydrated salts mixture (1DHPD:1SDH) as PCM

Figure 3. SEM images of (1DHPD:1SDH)/HNTs nanocontainer composite at the loading percentage of: a) pure HNTs, b) 58wt%, c) 70wt%, d) 82wt%, e) 88wt% PCM. Circles indicate unloaded PCMs

Figure 4. Melting enthalpies of (1DHPD:1SDH)/HNTs composites with various loadings vs. numbers of heat uptake/release cycles

Figure 5. a) Thermal cycling tests of hydrated salts mixture (1DHPD:1SDH) for 50 cycles, b) (1DHPD:1SDH)/HNTs nanocontainer composite for 50 cycles

Figure 6. Photos of hydrated salts mixture (1DHPD:1SDH) before a) and after b) heating, (1DHPD:1SDH)/HNTs composite before c) and after d) heating at 60 ˚C

Figure 7. TEM images of a) HNTs, c) PCM-loaded HNTs, EDX spectra of b) HNTs, d) PCM-loaded HNTs

Figure 8. FTIR spectra of hydrated salts mixture (1DHPD:1SDH), (1DHPD:1SDH)/HNTs nanocontainer composite and pure HNTs

Figure 9. XRD patterns of hydrated salts mixture (1DHPD:1SDH), HNTs and (1DHPD: 1SDH)/HNTs nanocontainer composite before and after heating at 60 °C